Research in Astron. Astrophys. **2009** Vol. **9** No. **1**, 11 – 40
http://www.raa-journal.org *http://www.iop.org/journals/raa*

Research in Astronomy and Astrophysics

INVITED REVIEWS

High energy neutron and pion-decay gamma-ray emissions from solar flares

Edward L. Chupp[1] and James M. Ryan[2]

Physics Department and Space Science Center in the Institute for the Study of Earth Oceans and Space, University of New Hampshire; *edward.chupp@unh.edu, james.ryan@unh.edu*

Received 2008 November 5; accepted 2008 November 26

Abstract Solar flare gamma-ray emissions from energetic ions and electrons have been detected and measured to GeV energies since 1980. In addition, neutrons produced in solar flares with 100 MeV to GeV energies have been observed at the Earth. These emissions are produced by the highest energy ions and electrons accelerated at the Sun and they provide our only direct (albeit secondary) knowledge about the properties of the accelerator(s) acting in a solar flare. The solar flares, which have direct evidence for pion-decay gamma-rays, are unique and are the focus of this paper. We review our current knowledge of the highest energy solar emissions, and how the characteristics of the acceleration process are deduced from the observations. Results from the RHESSI, INTEGRAL and CORONAS missions will also be covered. The review will also cover the solar flare capabilities of the new mission, FERMI GAMMA RAY SPACE TELESCOPE, launched on 2008 June 11. Finally, we discuss the requirements for future missions to advance this vital area of solar flare physics.

Key words: Sun — Flares — Particle Acceleration-Meson Production

1 INTRODUCTION

We focus on solar flare events in which there exists clear evidence for meson production by the interaction of $>$180 MeV protons or ions with the solar atmosphere. The presence of these mesons is indicated by the detectable emission of neutral meson-decay gamma-rays. By inference, events where secondary neutrons at ground level are detected belong to this class of events, even though no data may be available for the attendant gamma-rays. A goal of such investigations is to determine the mechanism(s) that accelerate the ions and electrons to such energies. We review, in Section 2, the basic gamma-ray and neutron production mechanisms and in Section 3, the properties of several selected events with pion-decay gamma-ray emission, some of which provide evidence for high energy neutrons ($>$50 MeV) and possible relativistic electron acceleration to several hundred MeV. In Section 4 we briefly mention some proposals for the acceleration mechanisms. We also review, in Section 5, the capabilities of the LAT on FERMI (GRST) to extend these observations, and in Section 6, we suggest future observations that are necessary to further our understanding of these processes. The Appendix provides a list of the *Long Duration Gamma-Ray Flares* observed though 1991 and characterized by Ryan (2000) as those that have long term hard X-/gamma-ray and neutron emissions extending well after (hours) the impulsive phase. Several flares discussed below are from that list. We also include more recent high energy ion-rich flares (up through 2005).

[1] Professor of Physics Emeritus; [2] Professor of Physics, Director of Space Science Center

2 GAMMA-RAY AND NEUTRON PRODUCTION

It is useful to first review the origin of the radiation detected from solar flares. Accelerated protons and electrons produce several different forms of secondary radiation, as shown in Table 1. Their relative intensities depend on the particle energy spectra and composition and the composition of the solar atmosphere in which they interact (Ramaty & Mandzhvidze 1994). For example, for protons in the approximate range of 10 MeV to 50 MeV, inelastic scattering on ambient ^{20}Ne, ^{12}C or ^{16}O nuclei produces narrow de-excitation gamma-ray lines at 1.634 MeV, 4.428 MeV and 6.129 MeV, respectively. Many other narrow lines are present in the spectrum representing the composition of the solar atmosphere. Broad nuclear lines are produced by accelerated heavy nuclei such as ^{12}C, ^{14}N, ^{16}O, ^{20}Ne, ^{28}Si, ^{24}Mg, and ^{56}Fe (Share & Murphy 1999, 2000, 2006). These lines are broad because the center of mass has a large velocity relative to the observer.

Table 1 Radiation Mechanisms

Nuclear De-excitation Lines (e.g. 4.428 MeV, 6.129 MeV)
Neutron Capture Line (2.223 MeV Photosphere)
Positron Annihilation (0.511 MeV Line, Beta+Emitter)
Orthopositronium (Triplet – 3Gamma, Singlet – 2Gamma)
Neutral Meson Decay (Peak at 67.5 MeV)
Neutron Production (e.g., p + ^{4}He = p + n +^{3} He)
Electron Bremsstrahlung

Notes: For details see Ramaty & Mandzhavidze (1994)

If the accelerated protons or ions have energies above ∼10 MeV/nucleon, neutrons can be produced as well. Those neutrons which are directed toward the photosphere are slowed by scattering and some will be captured by hydrogen nuclei to produce the deuteron emitting gamma-ray at 2.223 MeV. For protons of energy above approximately 180 MeV, their interaction with ambient helium will produce charged and neutral mesons, the latter decaying into high energy gamma-rays with a Doppler-broadened spectrum peaking at 67.5 MeV. The accompanying charged pions decay to muons that in turn decay to electrons (and neutrinos) that radiate in the gamma-ray range. Accelerated nuclei also produce positron emitters through a variety of nuclear reactions with ambient nuclei; a typical example being the production of ^{11}C. The positrons then undergo annihilation with electrons through either singlet or triplet positronium states (i.e., spins opposite or aligned, respectively). In the former case, a pair of photons with energy 0.511 MeV emerges and in the latter case a continuum of photon energies emerges from the three gamma rays produced.

Accelerated primary electrons also undergo inelastic scattering yielding bremsstrahlung radiation with a broad energy spectrum extending up to the originating electron energy. Lin (2006) reviewed the hard X-ray and gamma-ray solar flare emissions observed below ∼10 MeV. See also Share & Murphy (2000) for a review of "Gamma-Ray Spectroscopy in the Pre-HESSI Era."

As mentioned above, meson production can occur from either proton-proton or proton-alpha interactions (with smaller contributions from higher Z reactions). The basic processes were investigated in detail by Murphy, Dermer & Ramaty (1987) and Table 2 shows the principle π-meson production reactions they considered.

Figure 1 shows the cross-section for proton-proton (p-p) interactions producing charged and neutral mesons and neutrons as indicated in Table 2 for reactions 1–4. Reaction 1 for neutral meson (π^0) production has a threshold of 270 MeV. Figure 2 shows the neutral-meson decay gamma-ray spectrum for mono-energetic p-p reactions.

For the events that we discuss below, the shape of the meson-decay gamma-ray spectrum is sensitive to the form of the proton spectrum. For example, if the proton energy is just above 300 MeV, the narrow, neutral-meson decay gamma-ray spectrum, shown in Figure 2, will ride on top of the bremsstrahlung continuum deriving from the $\pi^{\pm}$ decay. As the proton energy increases (Fig. 2), the broader decay

Table 2 Reactions of Protons and Alpha Particles Involving Pions

Reaction Number	Reaction	Reaction Number	Reaction
1	$p + p \rightarrow \pi^0 + X$	6	$p + \alpha \rightarrow \pi^0 + X$
2	$p + p \rightarrow \pi^+ + X$	7	$p + \alpha \rightarrow \pi^+ + X$
3	$p + p \rightarrow \pi^- + X$	8	$p + \alpha \rightarrow \pi^- + X$
4	$p + p \rightarrow n + X$	9	$p + \alpha \rightarrow n + X$
5	$p + p \rightarrow p + X$ (inelastic)	10	$p + \alpha \rightarrow p + X$ (inelastic)

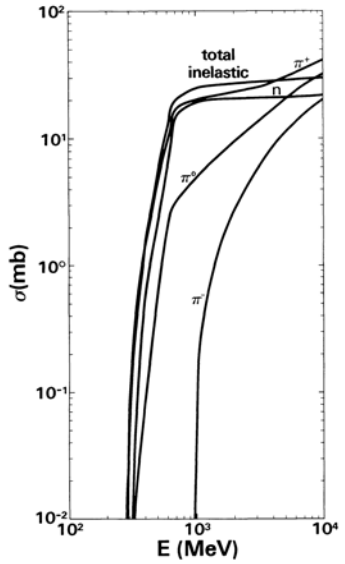

Fig. 1 Cross-section for p-p reactions. From Murphy, Dermer & Ramaty (1987), ApJS 63, 721. Reproduced by permission of AAS.

spectrum produces a flattening of the composite spectrum. Alexander & MacKinnon (1993) considered this effect for proton-proton interactions, as discussed below in Section 5. If protons interact with alpha particles, neutral mesons are produced at lower energies, so the resulting photon spectrum also depends on the ratio of proton/alpha particles.

The Primakoff effect, i.e., the production of pions by high energy photons, is not of practical interest for the solar flare case (see Primakoff 1951; Halprin et al. 1966).

3 SELECTED EVENTS

Morrison (1958) predicted that nuclear reactions from accelerated particle interactions in the solar atmosphere during a solar flare could produce a neutron-proton capture line at 2.223 MeV detectable at the Earth. Later Lingenfelter & Ramaty (1967) computed the expected emission of gamma-ray lines, continuum and high energy neutrons produced during a solar flare. These early predictions were confirmed during a series of solar flares in August 1972 with the Gamma-Ray Monitor on the OSO-7 spacecraft (Chupp et al. 1973). The detections of the neutrons at the Earth and the higher energy gamma-rays resulting from the decay of neutral pions, was yet to come. The ability to detect and measure high-energy photons and neutrons came with the Solar Maximum Mission that carried on the Gamma Ray Spectrometer. The SMM repair mission by the ill-fated Challenger space shuttle on 1984 April 6 enabled the GRS to record many more solar flare and gamma-ray burst events until its planned demise

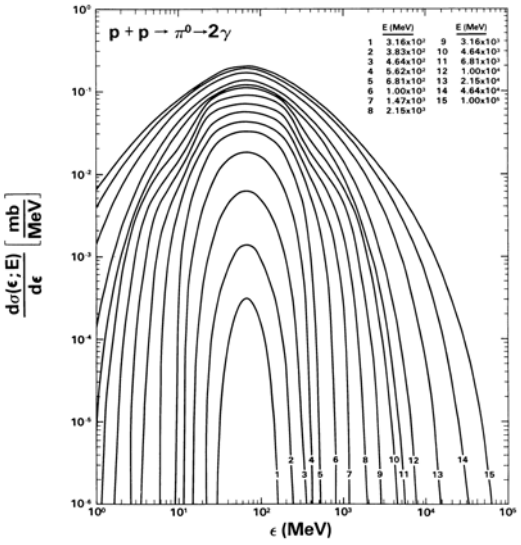

Fig. 2 The neutral meson decay gamma-ray spectrum for mono-energetic p-p reactions. From Murphy, Dermer & Ramaty (1987), ApJS 63, 721. Reproduced by permission of AAS.

on 1989 December 2 over the Indian Ocean. From the SMM launch on Valetine's day in 1980, nearly ten years of operation provided the high-energy solar physics community with many exciting events to study (Vestrand et al. 1999).

Several events illustrate the phenomena associated with high-energy particle production in flares. In choosing these events to highlight and study, we have avoided events where the energetic particles arise from interplanetary acceleration processes. The events we have chosen show clear neutral particle signatures, even though interplanetary and GLE particles were present. Later, we address the question of possible connections between these detected particles and the neutral particle signatures. In later sections, we discuss events we suspect were, in fact, high-energy events, but no instrumentation was capable of registering or measuring that radiation.

3.1 1982 June 3

The first convincing observations of meson production in a solar flare, as measured by the SMM/GRS, were reported by Forrest et al. (1985). A 2B (X8.0) white light flare occurred at E72S09 (72 ° HCA) in McMath Region 3763. The flare exhibited an intense impulsive phase, like many others before it, but also an extended phase that would later be associated with unusual high-energy emission. In Figure 3, panels b, c and d show the average background-subtracted time-integrated spectra for photon energies of 10–140 MeV. The individual spectra represent the impulsive phase, early in the extended phase, and late in the extended phase when the effects of neutrons arriving at the spacecraft are evident. The horizontal bars show the energy range for binning the differential fluence (photons cm $^{-2}$ MeV^{-1}), and the vertical bars show the 1-sigma errors in the fluence. The lower three curves show fits to the average fluence curve, i.e., a π^0-decay gamma-ray spectrum, a $\pi^+ \rightarrow \mu^+ \rightarrow e^+$ decay bremsstrahlung spectrum, and their sum. Panel (c) shows that the sum of the two meson decay components is a satisfactory fit to the full flare, time-integrated spectrum, characterized by a significant flattening below about 70 MeV.

We note that panel (a) in Figure 3 shows the SMM/GRS high-energy loss spectrum during the 1980 June 21 solar flare. This was actually the first event to exhibit detectable high-energy gamma-ray and neutron emission (Chupp et al. 1982). The spectrum shown is believed to be mostly constituted of bremsstrahlung from relativistic electrons, and even though pions were likely produced (inferred from

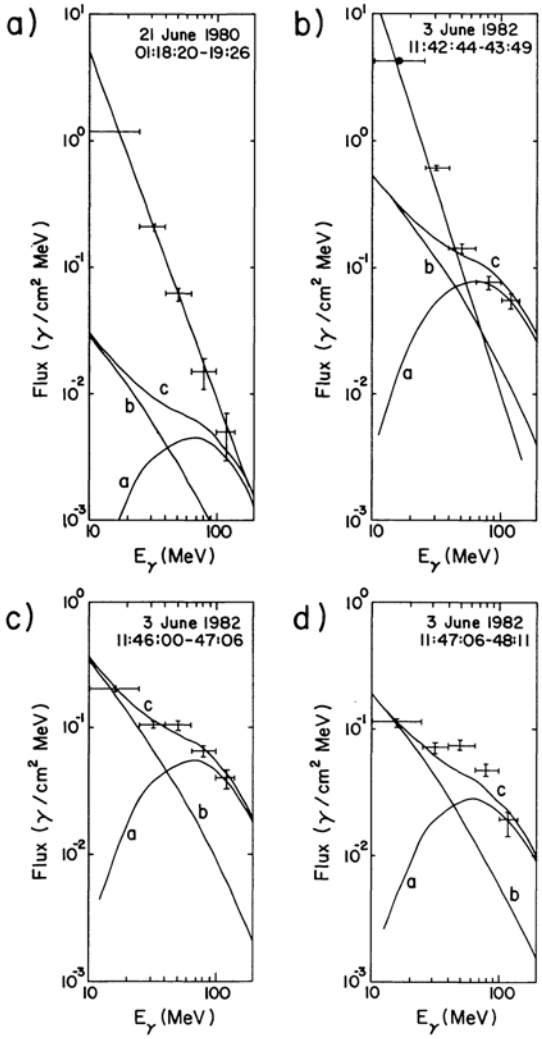

Fig. 3 Panel (a) shows the SMM/GRS high-energy loss spectrum during the 1980 June 21 solar flare. Panels (b), (c), (d) show the average background-subtracted time-integrated spectra for photon energies of 10–140 MeV for the 1982 June 3 solar flare. From Chupp (1990) ApJ 73, 213, and based on Forrest et al. (1985). Reproduced by permission of AAS.

the secondary neutron energies) the event is not included in our list. See also Rieger (1994), Rieger, Gan & Marschhäuser (1998) and Gan & Rieger (1999).

The 1982 June 3 flare also provided clear signals of neutron production extending in energy to over 1 GeV with sufficient intensity to be recorded by neutron monitors at mountain altitudes. The time-intensity profile of the event in several SMM/GRS energy channels is shown in Figure 4 with the GRS rates (>25 MeV) arising from the combination of high-energy photons and high-energy neutrons. The lower curve shows the response of the Jungfraujoch neutron monitor during the event. The total neutron emissivity toward the Earth was estimated assuming that this quantity tracks the π^0 meson intensity throughout the event. The result is shown in Figure 5.

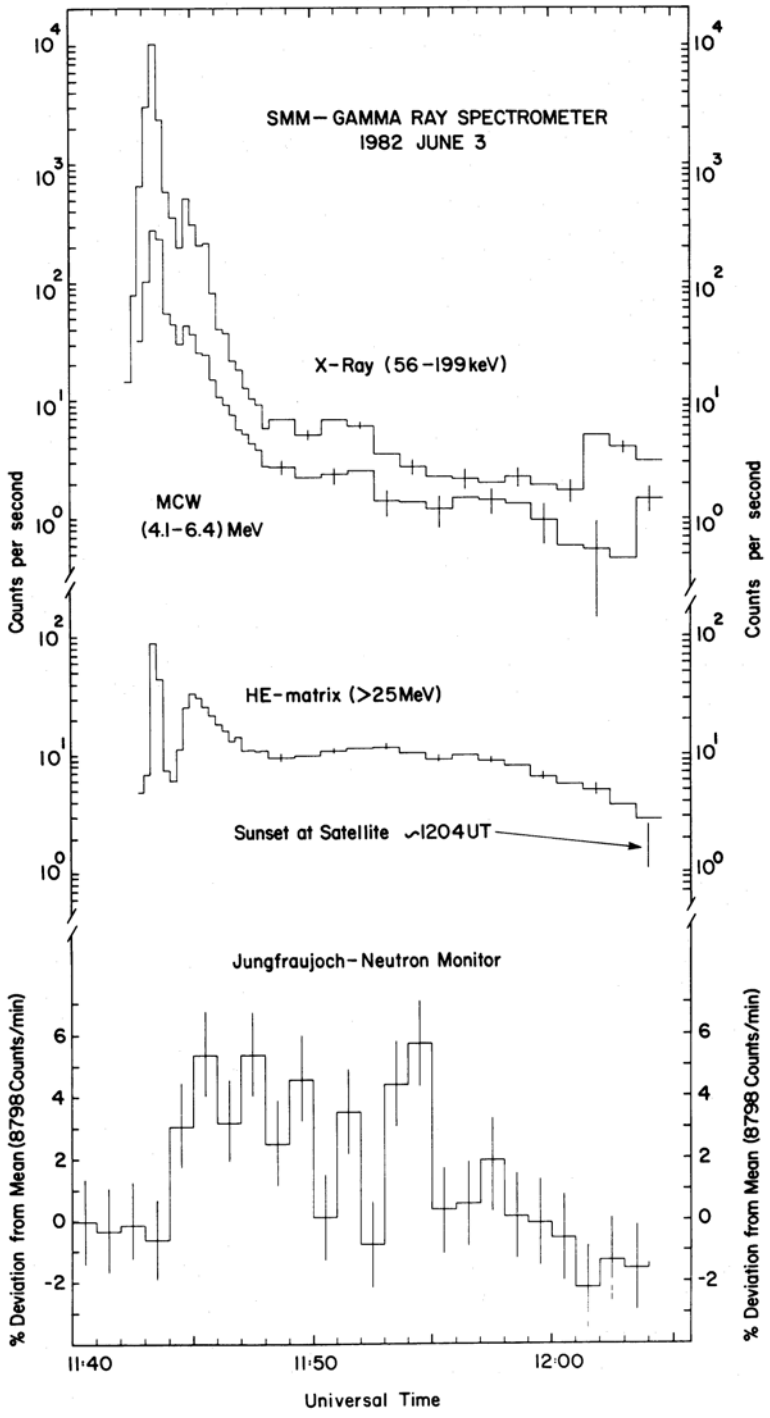

Fig. 4 Time histories of several data channels during the 1982 June 3 Solar Flare. From Chupp et al. (1987), ApJ 318, 913. Reproduced by permission of AAS.

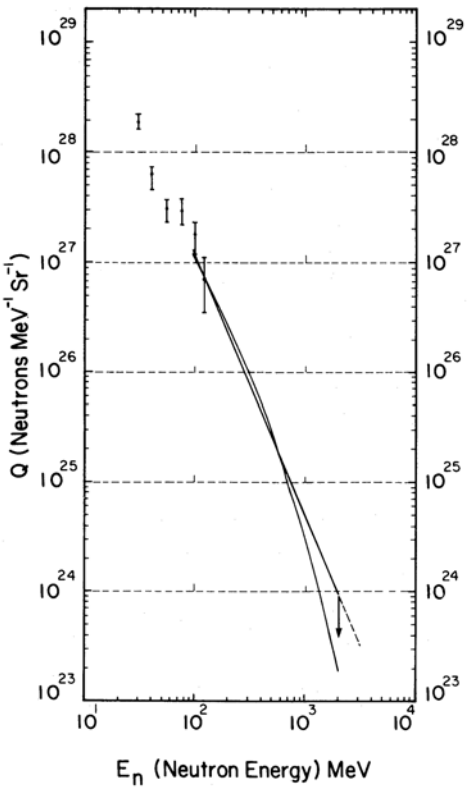

Fig. 5 The time-integrated directional neutron emissivity. Data points from neutron decay proton observations from Evenson et al. (1983) are shown below 100 MeV. From Chupp et al. (1987), ApJ 318, 913. Reproduced by permission of AAS.

3.2 1989 March 6

One of longest duration flare events was that of 1989 March 6, starting in X-rays at 1350 UT. The flare from NOAA/SESC active region 5359 saturated the GOES X-ray detectors and was estimated as X15 with a 3B Hα classification. Rieger et al. (1999) concluded that 2.22 MeV line emission was observed after 13:57:46 UT and nuclear line emission of varying intensity was observed throughout the flare. The total measured fluence of this line was at least 177 ± 20 photons cm^{-2} from 13:56 – 14:53 UT (3420 s). This can be compared to the total measured fluence of this line during the 1982 June 3 flare of at least 204 photons cm^{-2} over a period of 1200 s. These values are not corrected for the angular distribution of the emitted photons. For more details, see Rieger (1998) and Hua & Lingenfelter (1987). Several studies of the first four minutes of the flare concluded that the three initial short hard X-ray/gamma-ray bursts of duration 98 s, 4 s and 131 s, respectively, were dominated by electron bremsstrahlung with intense emission above 10 MeV and a roll over below 60 MeV (see Rieger & Marschhäuser 1990; Marschhäuser, Rieger & Kanbach 1994; Rieger, Gan & Marschhäuser 1998).

After the first burst, from 1358:40 UT to 1359:05 UT, the Ondřejov radio spectrometer recorded weak radio emission between (700 – 1000) MHz. According to a personal communication with Rieger et al. (1999) from M. Poquérusse, the Nançay radio spectrometer showed only narrow band bursts between (150–250) MHz, but after 1358:40 UT, a group of U-bursts extending from about 1100 MHz down to below 900 MHz was observed. After 1401 UT, an intense Type II burst developed in the (200 – 400) MHz range. To explain these observations, Rieger et al. (1999) used a modified Heyvaerts, Priest

& Rust (1997) emerging flux model. This model envisages a low lying, dense, closed loop that interacts with a new emerging loop of opposing polarity. Reconnection takes place and no open field line exists. Accelerated electrons and ions lie on closed field lines and produce the early hard X-ray emission, but in the initial energy release phase, the closed loop system is presumed to be so low that the confined particle beams cannot escape to the upper corona. This is the authors' explanation for the lack of Type III emission. The presence of U bursts after the first impulsive emission and their decreasing low frequency cut-off with time indicates that the later electron beams are still injected into a closed field configuration.

Before 1401 UT, because of the presence of nuclear line emission, proton and ion acceleration to 50 MeV occurred in the first four minutes of the flare. The contribution to the nuclear emission from heavy ions is uncertain. Evidence for meson-decay gamma-ray production from 1403 UT to 1410 UT was reported by Dunphy & Chupp (1991). This emission requires protons of energy greater than 300 MeV for p-p interactions, or alpha particles with energy greater than 180 MeV for p-α interactions.

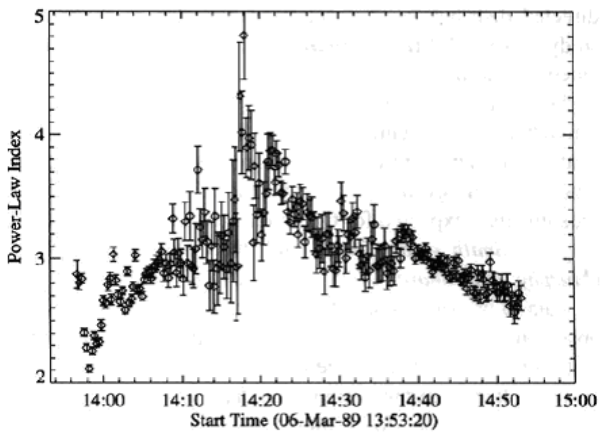

Fig. 6 Temporal Variation of the bremsstrahlung power-law index during the 1989 March 6 flare. From Share & Murphy (2006), in AGU Geophysical Monograph Series 165, 177. Copyright 2006 American Geophysical Union. Reproduced by permission of American Geophysical Union.

This flare is unique in that it does not simply behave like other LDGRFs. Figure 6 shows the index of the power-law fit to the bremsstrahlung spectrum in the SMM/GRS main channel from 0.3–8 MeV (Share & Murphy 2006). From the beginning of the flare until 1406 UT, the spectrum is hard as discussed above, but then undergoes a sudden softening at 14:20 UT for several minutes followed by progressive hardening until the end of the flare. At this time, it is likely that several steep bursts of electron bremsstrahlung occurred, but the full analysis of the flare is incomplete. This general behavior was to be repeated two years later and observed with the Compton Gamma Ray Observatory. It was also reminiscent in many ways of the 1982 June 3 event with two distinct phases.

3.3 1990 May 24

After the end of the SMM mission, the community expected that the COMPTON GAMMA RAY OBSERVATORY would continue solar flare observations, but the Challenger accident of 1986 January 28 postponed that mission until 1991. Fortuitously, there were two high-energy gamma-ray detectors in orbit: the PHEBUS spectrometer on the GRANAT spacecraft and the GAMMA-1 spectrometer on the Gamma Satellite (see Sect. 3.4). The GRANAT satellite was launched from Baikonor on 1989 December 1.

The 1990 May 24 GOES X9.3 flare at N36W76 was well observed with PHEBUS. PHEBUS consisted of two BGO crystals designed to record transient photon events in the energy range 100 keV–

100 MeV. Preliminary analyses of the flare were reviewed by Ryan (2000). More recently, Vilmer et al. (2003) re-examined the early interpretations of this event emphasizing the evidence for pion decay radiation.

Figure 7 shows the intensity-time profiles of three high-energy channels sensitive to energies greater than 10 MeV. The impulsive phase occurred from 2047:50 UT to 2049:24 UT, with high energy emission above 75 MeV present up to and beyond the end of observations at 2057 UT. By this time, very energetic neutrons >500 MeV, had already arrived at GRANAT (Debrunner et al. 1993; Debrunner et al. 1997). They found the number of neutrons >100 MeV, ejected from the Sun to the Earth, as $<1.1\times10^{30}$ sr^{-1}, compared to 8×10^{32} sr^{-1} for the 1982 June 3 Solar flare (Chupp et al. 1987, see also Koval'tsov et al. 1994). For a review of the direct neutrons observed by the Climax Neutron Monitor see Kocharov et al. (1994a). Vilmer et al. (2003) focused on the time period before the arrival of the high energy neutrons from 2047:50 UT to 2050:10 UT.

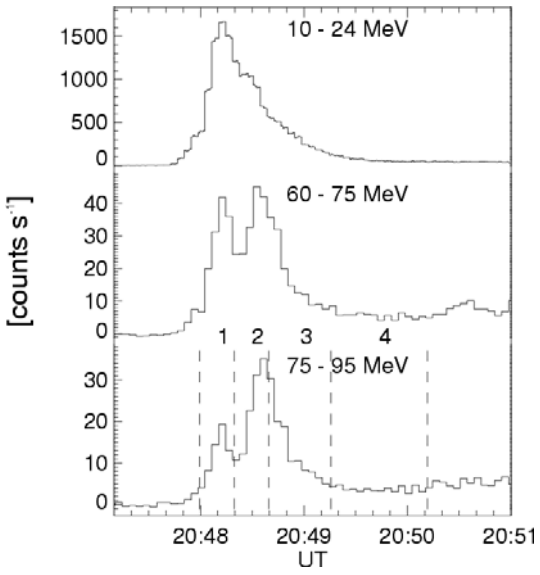

Fig. 7 The time histories of three energy loss channels above 10 MeV, and four time intervals for spectral analysis are shown. From Vilmer et al. (2003), A&A 412, 865. Copyright A&A Editor in Chief, Claude Bertout, Permission granted for reproduction.

In Figure 8, background subtracted count spectra are shown for the four time intervals indicated in Figure 7 with energy channel widths and error bars (only visible for spectrum 4). The curves show best fits for several combinations of electron bremsstrahlung and π^0 and π^+ meson-decay gamma-radiation. Vilmer et al. (2003) concluded that including pion-decay radiation only improves the fits for spectra 2, 3 and 4, confirming the earlier analysis of Debrunner, Lockwood & Ryan (1993) and Debrunner et al. (1997). Actually, the relative contribution of pion decay radiation increases with time, consistent with the general pattern of LDGRFs. Because PHEBUS only measured the spectrum of photons up to 100 MeV, the primary proton spectra used in the modeling was not well determined (Vilmer et al. 2003).

The background-subtracted photon count spectrum from 300 keV to 100 MeV during the fourth time interval (2049:15.648 UT to 2050:11.648 UT) is shown in Figure 9. The solid curve is the best fit for the combined single bremsstrahlung and pion decay components. Vilmer et al. (2003) reported the electron bremsstrahlung component as the dotted curve. The excess counts above this curve are then due to nuclear gamma-rays at 2.2 MeV and the broad components in the energy interval 3.7–7.6 MeV.

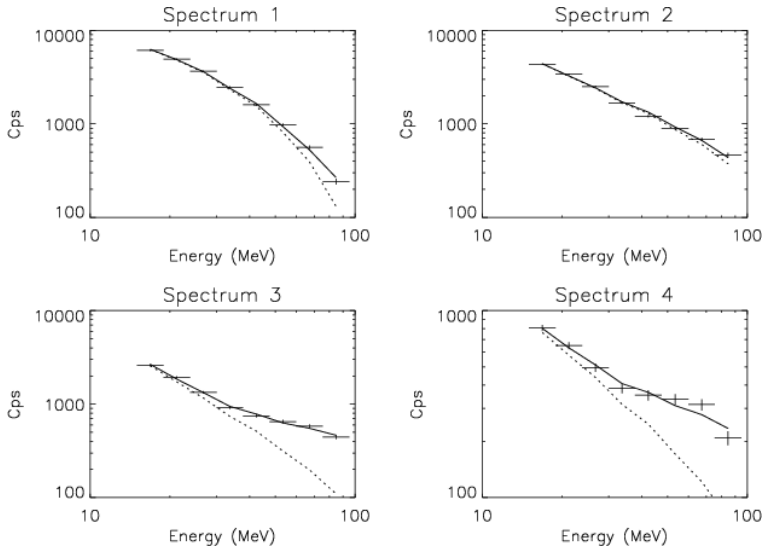

Fig. 8 Background subtracted count spectra observed by PHEBUS/GRANAT during time intervals 1–4 in the (10–100) MeV energy range. The full line indicates one of the best fits found above 10 MeV for an electron bremsstrahlung component and a pion contribution. The dotted line shows only the electron bremsstrahlung component. From Vilmer et al. (2003), A&A 412, 865. Copyright A&A Editor in Chief, Claude Bertout, Permission granted for reproduction.

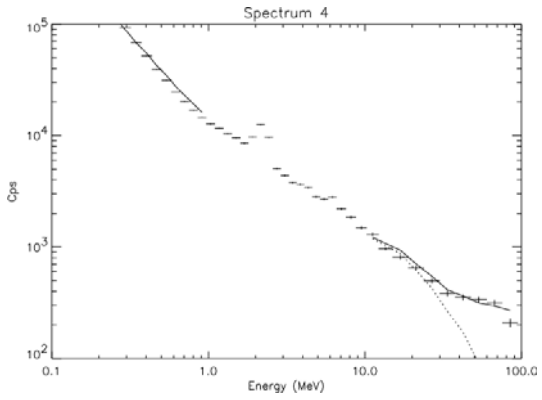

Fig. 9 Background subtracted count spectrum for the fourth time interval from 300 keV to 100 MeV. From Vilmer et al. (2003), A&A 412, 865. Copyright A&A Editor in Chief, Claude Bertout. Permission granted for reproduction.

The 1990 May 24 flare also provides a dramatic example of the characteristic property that distinguishes flares with pion production from those with only nuclear line production. Figure 10 (Ryan 2000) shows the time-dependent ratio of the (70–94) MeV photon emission to the (4–7) MeV nuclear emission for the full observable emissions. The sudden increase of this ratio about 2–3 minutes after the flare illustrates the presence of the proton (ion) acceleration to several hundred MeV. Ryan (2000) emphasized that the smooth decay of the count rate at high energies is consistent with prolonged quasi-steady emission rather than to "numerous small episodes of acceleration".

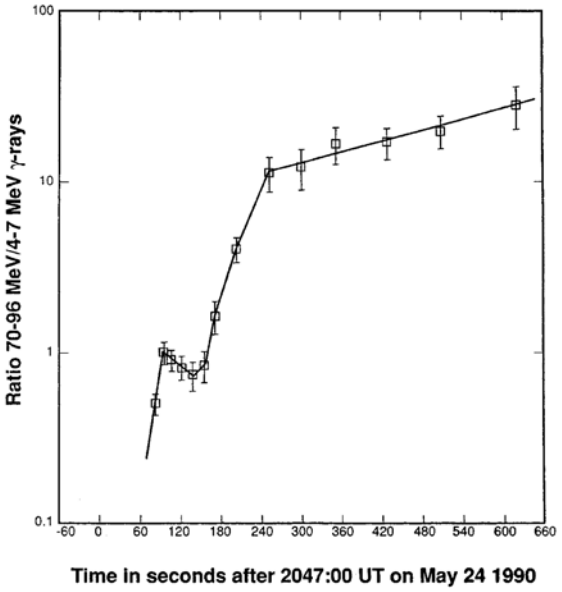

Fig. 10 The time-dependent ratio of the 70–94 MeV photon emission to the 4–7 MeV nuclear emission for the full observable emissions. Space Science Reviews (2000), LONG-DURATION SOLAR GAMMA-RAY FLARES by, James M. Ryan, 93, 581–610; Figure 4, page 592. With kind permission from Springer Science and Business Media.

3.4 1991 March 26

The Gamma Observatory was a Soviet spacecraft launched on 1990 July 11. It carried the GAMMA-1 telescope, the disk-M telescope and the Pulsar X-2 telescope. Shortly after launch, the power to the spark chamber failed so only the GAMMA-1 telescope could operate; its scintillation counters covering the energy range 50 MeV –6 GeV. The mission lasted two years and overlapped the first year of the CGRO mission (see Sect. 3.6 below).

The GAMMA-1 telescope registered high energy gamma rays from the two-ribbon 3B/X4.7 white light flare on 1991 March 26 (Akimov et al. 1994). Apparently, this flare was only observed in soft X-rays by the GOES satellite. No higher energy (>12 keV) X-ray observation was available. GAMMA-1 only recorded photons above 30 MeV. Figure 11 shows that the high energy gamma rays first appear just before 2028 UT. Akimov et al. (1994) measured differential gamma-ray spectra for the "impulsive interval 2027:07–2028:07 UT" up to 300 MeV and the "trailer interval 2028:07-2029:20 UT" up to 200 MeV. They noted that the latter spectrum is steeper, consistent with the early phase of many X-ray/gamma-ray flares. This early phase is interpreted as due to primary electron-bremsstrahlung in a dense medium with $n \approx 10^{14}$ cm^{-3}.

The gamma-ray intensity-time profile below and above 100 MeV is shown in Figure 12 for the full observing period. A delayed enhancement of the >100 MeV component is apparent about 8 minutes after the flare onset. Because of limited count statistics, a spectral ratio $R = N(<100\,\text{MeV})/N(>100\,\text{MeV})$ was computed for the impulsive and delayed components, respectively, yielding values of 1.1 and 0.2 . The difference was stated to be at the 4σ confidence level. This delayed hardening of the higher-energy photons is consistent with the production of meson-decay gamma rays. The 9.5 GHz microwave emission, shown also in Figure 12, indicates a delayed release of energy at the time of the >100 eV photons increase. The flare on 1991 June 15, discussed below and also observed by GAMMA-1, shows a similar behavior.

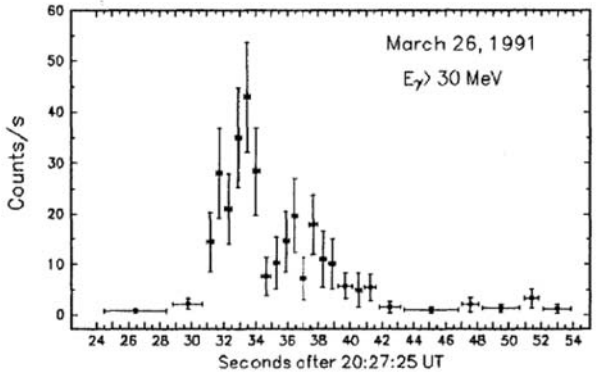

Fig. 11 The early time history above the GAMMA-1 threshold of 30 MeV. Reprinted with permission from, Akimov et al. (1994), AIP Conf. Proc. 294, 130–133; Figure 1, page 131. Copyright 1994, American Institute of Physics.

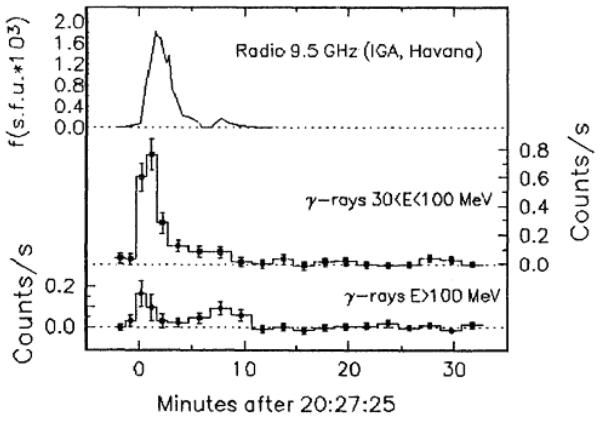

Fig. 12 The full time history above the GAMMA-1 threshold of 30 MeV in two energy intervals. Reprinted with permission from, Akimov et al. (1994), AIP Conf. Proc. 294, 130–133; figure 3, page 132. Copyright 1994, America Institute of Physics.

3.5 1991 June 11 (01:56 UT)

The Compton Gamma Ray Observatory (CGRO), named in honor of Dr. Arthur Holly Compton, was launched on 1991 April 5 and re-entered the Earth's atmosphere on 2000 June 4, after a planned de-orbit maneuver. CGRO carried four instruments covering the photon energy range 30 keV–30 GeV; BATSE, OSSE, COMPTEL and EGRET, in order of increasing energy. The best example of a meson-decay gamma ray event is the 1991 June 11 flare that occurred in NOAA active region 6659, commencing at 0156 UT in Hα. CGRO observations were made by the EGRET spark chamber and its NaI calorimeter (TASC) that registered meson-decay gamma rays and electron bremsstrahlung to >1 GeV (Kanbach et al. 1993). The TASC also registered high-energy neutrons (Dunphy et al. 1999). The COMPTEL telescope recorded the 2.223 MeV line emission for five hours (Rank 1996; Rank et al. 1996; Rank et al. 2001). The OSSE spectrometer observed several gamma-ray lines and continuum to >16 MeV

(Murphy & Share 2000). In addition, the PHEBUS spectrometer on GRANAT observed gamma-ray lines and continuum to 100 MeV (Trottet et al. 1993).

The EGRET and TASC observations show that the first impulsive emissions included intense "prompt" nuclear lines and the extended emissions included strong – long lasting (8 hrs) – meson decay gamma rays, especially from π^{o} decay, indicating a strong interacting flux of protons with energies >300 MeV (Kanbach et al. 1993). Gamma-rays extending in energy to $\sim$ 2 GeV were also detected during the extended emission phase, probably from extreme energy relativistic electron bremsstrahlung and/or neutral pion decay.

Figure 13 shows the emissions above 50 MeV as recorded by the EGRET. The spark chamber deadtime loss was 100% before 0340 UT, so only the rate after this time is shown. Kanbach et al. (1993) fit two components to this time profile—a fast decay between 0330 to 0500 UT, with a time constant of 25 minutes and a slow decay with a time constant of 255 minutes.

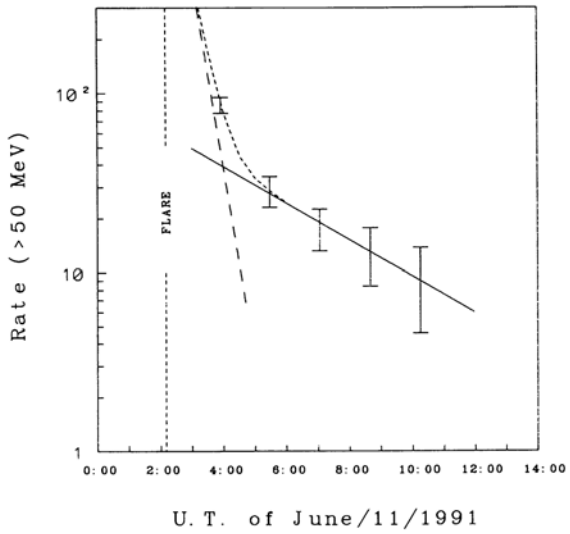

Fig. 13 The time profile of the solar emission >50 MeV on 1991 June 11. From Kanbach et al. (1993), A&AS 97, 349. Copyright A&A Editor in Chief, Claude Bertout, Permission granted for reproduction.

Figure 14 shows the measured photon spectrum between 0326 and 0600 UT. The theoretical spectrum shown was reported by Mandzhavidze & Ramaty (1992) and Ramaty et al. (1992). Their initial interpretation was that there was a considerable primary electron bremsstrahlung component, but this was later refuted by Rank et al. (2001) who attributed the entire emission during the extended phase to nuclear processes. Mandzhavidze and Ramaty (1992) derived a pion-generated gamma-ray spectrum from proton power-law spectra used to explain the GAMMA-1 observations of another disk flare on 1991 June 15 (Akimov et al. 1991, see below). The resulting gamma-ray spectra from power laws, $s = 3$ and 4 were normalized at about 300 MeV photon energy. Kanbach et al. (1993) also pointed out that these spectra show that the radiation between 200 MeV and 2 GeV can be completely described by π^0 radiation!

Of particular interest is the question of whether the long lasting high energy gamma-ray emission is caused by continuous acceleration of the protons above $\sim$ 300 MeV, as discussed by Ryan & Lee (1991) in the context of the 1982 June 3 flare, or by the injection of flare accelerated particles into a large coronal loop with release to the mirror points of the loop where the gamma-rays are produced. Kanbach et al. (1993) concluded that the protons must be trapped in a storage region that extends to a height above 5×10^8 cm (7×10^{-3} $R_\odot$). Also, pitch angle scattering must be absent for the high energy

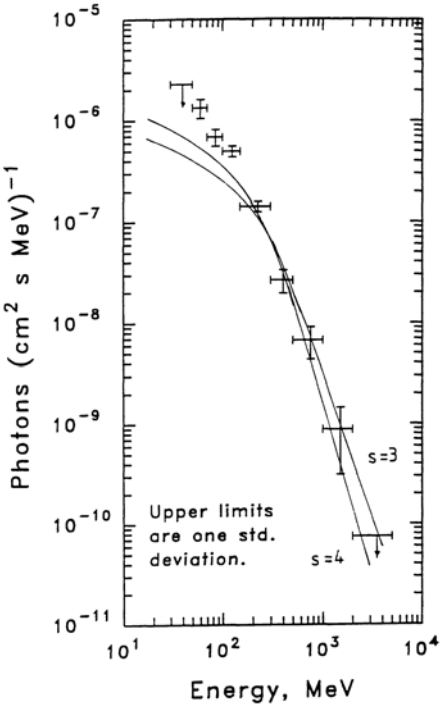

Fig. 14 The gamma-ray energy spectrum for the 1991 June 11 Solar Flare is shown for several energy channels by the data points. The curves are discussed in the text. From Kanbach et al. (1993), A&AS 97, 349 (Copyright A&A Editor in Chief, Claude Bertout, Permission granted for reproduction).

emission to last several hours. Furthermore, Dunphy et al. (1999) showed that the EGRET/TASC data during the extended emission was also consistent with the presence of a flux of high-energy neutrons near the Earth!

3.6 1991 June 15

Gamma-rays with energy above 1 GeV were also detected with the GAMMA-1 telescope during the 3B-X12 1991 June 15 (Akimov et al. 1991). During the beginning of the flare in GOES 7 (1–8 Å) X-rays starting at 0810 UT, the GAMMA-1 telescope was turned off and behind the Earth. When the instrument was turned on at 0837:22 UT, it recorded a flux of photons up to 4×10^{-3} cm^{-2} s^{-1} above 100 MeV. While this flux decayed in intensity, the photon spectral shape remained the same for $\sim$ 23 minutes. Figure 15 shows the background-subtracted count rate for the gamma-ray emission above 100 MeV, the later (1–10 MeV) gamma-rays as observed by COMPTEL (Ryan et al. 1993; McConnell et al. 1993), and the 5.2 GHz microwave flux density as recorded at the IAP (Bern) fixed frequency radiometer. Akimov et al. (1996) argued that the delayed post burst radio emission shown in Figure 15, which has 100–200 s sub-bursts, suggests dynamic energy release during the post-loop formation phase seen in Hα.

The best fit average de-convolved GAMMA-1 gamma-ray spectrum during the first orbit of GAMMA is shown in Figure 16. The spectral shape with a maximum in the 70–100 MeV energy range is consistent with the decay of neutral mesons.

The multiwavelength study of this event by Akimov et al. (1996), led to the conclusion that a prolonged acceleration *(and not simply long term trapping of energetic electrons and ions)* of protons to GeV energies is responsible for the long term gamma-ray emission. Note that this view contrasts with

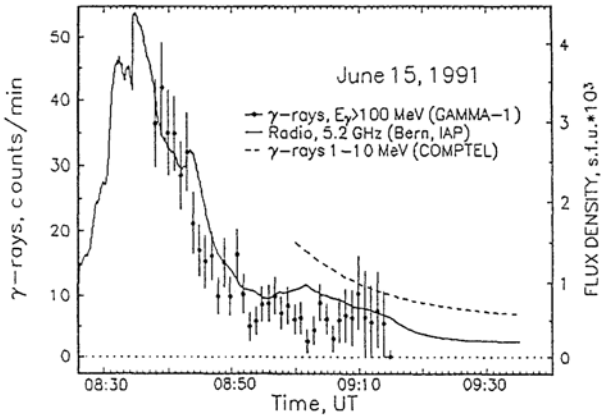

Fig. 15 The background-subtracted count rate for the gamma-ray emission above 100 MeV, the later (1–10 MeV) gamma-rays as observed by COMPTEL, and the 5.2 GHz microwave flux density as recorded at the IAP (Bern) fixed frequency radiometer. From Akimov et al. (1996), Solar Physics 166, 107–134; Figure 5, page 116. With kind permission from Springer Science and Business Media.

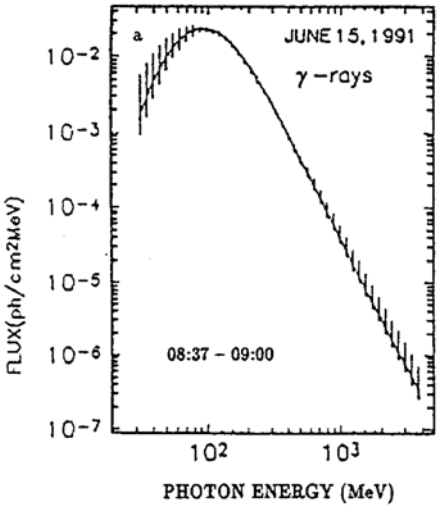

Fig. 16 The best fit average de-convolved GAMMA-1 gamma-ray spectrum during the first orbit of GAMMA. From Akimov et al. (1996), Solar Physics 166, 107–134; figure 8a, page 122. With kind permission from Springer Science and Business Media.

the picture presented by Kanbach et al. (1993) to explain the extremely long term emission observed in the 1991 June 11 flare; i.e., protons are trapped in a storage region at a coronal height greater than 5×10^8 cm ($7\times10^{-3}\ R_\odot$). Kocharov et al. (1994b) also concluded that continuous acceleration is also a natural explanation for the gradual phase of this flare. Kocharov et al. (1998) made a further study of this flare, comparing COMPTEL and GAMMA-1 spectra finding that the spectrum must first steepen ($>$100 MeV) and then harden to produce observable GeV photons. They further concluded, because of the low neutron intensity, that the particles responsible for producing the neutrons were relatively deficient in high-Z ions.

Mandzhavidze & Ramaty (1992) and Ramaty et al. (1992), in analyzing the 1991 June 11 flare, derived pion-generated gamma-ray spectra from proton power-law spectra used to fit the GAMMA-1 observations on 1991 June 15 (see Fig. 14 and the related discussion).

3.7 2003 October 28 (before 1101 UT)

The end of the Twentieth Century should have seen the launch of the High Energy Solar Spectroscopic Imager (HESSI) in July 2000, however the satellite was damaged during vibration testing, missing the peak of activity for Solar Cycle 23. The successful launch took place on 2002 February 5 from the belly of an Orbital Sciences Corporation plane over the Atlantic Ocean. Since then, several significant solar flares were measured and recorded during the remainder of the cycle. The satellite is now known as the Ramaty High Energy Spectroscopic Imager (RHESSI) in honor of the late Reuven Ramaty a leader in theoretical high-energy solar physics. The launch of the Coronas-F satellite, on 2001 July 31, by Russia, carrying the SONG Gamma Emission Spectrometer has provided additional data at gamma-ray energies above the RHESSI limit of 17 MeV.

The GOES class X17 Flare from the NOAA Active Region, 10486 at S16E08,was observed by RHESSI (Hurford et al. 2006) and the INTEGRAL/SPI (Kiener et al. 2006). The X-ray emissions observed by the GOES satellites began at 0941 UT, until 1124 UT with a maximum at 1110 UT, while the various INTEGRAL detectors recorded the event from about 1102 UT. The RHESSI observations began at ∼1106 UT and continued until about 1130 UT. These observations were summarized by Hurford et al. (2006) and are shown in Figure 17.

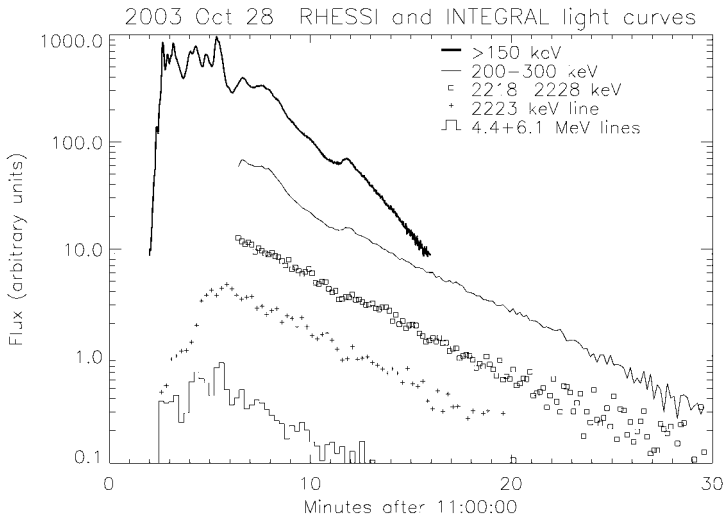

Fig. 17 Gamma-ray light curves for the 2003 October 28 event from RHESSI and INTEGRAL/SPI data adapted from Kiener et al. (2006), are shown in the top curve and the two lowest curves. The top curve is the dead-time corrected shield count rate that responds to >150 keV photons. The other curves have been corrected for pre- or postflare levels of background. Line fluences have been corrected for continuum emission. For clarity, the ordinate for each curve has been shifted by an arbitrary factor. From Hurford et al. (2006) ApJ 644, L94. Reproduced by permission of AAS.

Share & Murphy (2006), at the Chapman Conference also discuss several aspects of this flare, such as the hardening of the bremsstrahlung spectrum above 1 MeV which they suggest may be due to the decay of the charged pions which leads to the production of positonium. Of course, this requires the presence of meson-decay gamma rays in this 2003 October 28 flare.

In addition, the SONG spectrometer on the CORONAS spacecraft observed the flare (Kuznetsov et al. 2005; Kuznetsov et al. 2006; Miroshnichenko et al. 2005). Figure 18 (personal communication from V. G. Kurt to E. L. Chupp) shows the SONG neutron count rates (s^{-1}) with 40–60 and 60–90 MeV energy deposition and gamma-ray count rate (s^{-1}) in the same two energy intervals in RED. The (40–60 MeV) gamma-ray increase begins at ∼1102:11 UT and the (60–90 MeV) at ∼1103:40 UT, as shown in the lower and middle panels, respectively. The first increase is consistent with the INTEGRAL data shown in Figure 17, while the second heralds the onset of meson-decay gamma-ray production. The upper panel in Figure 18 shows the Tsumeb Neutron Monitor enhancement of 3.4 ± 0.3%, beginning at 1105–1106 UT. The inferred SONG neutron onset is 1106:20–1107:10 UT. Therefore, the confirmed production of several-hundred-MeV neutrons also implies the production of mesons. Hence, it is reasonable to believe that the increase in the (60–90 MeV) rate, shown in Figure 18, is due to the arrival of meson-decay gamma rays with peak energy of ∼70 MeV.

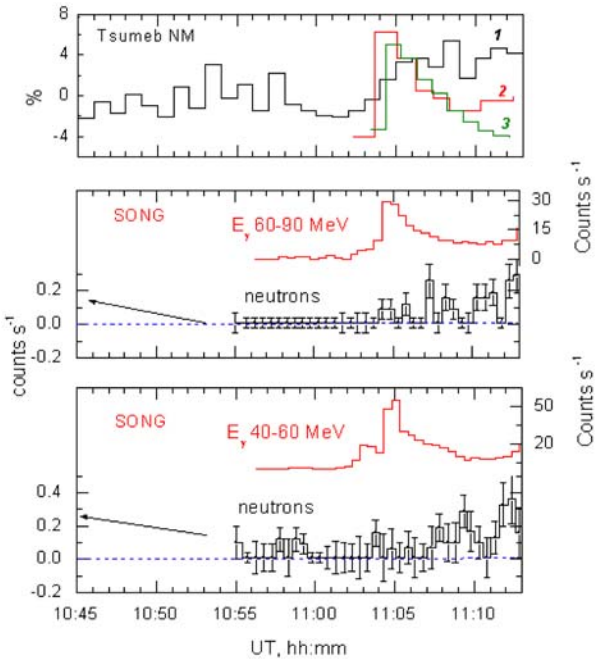

Fig. 18 SONG and Tsumeb (NM) count rates for the 2003 October 28 Solar Flare (personal communication from V. G. Kurt to E. L. Chupp).

Miroshnichenko et al. (2005) also made an extensive study of this event with emphasis on the neutron monitor observations and the propagation of the protons and electrons to the Earth. Figure 19 shows the five-minute summed percentage deviations from the mean for the South Africa Tsumeb neutron monitor at 20S/18E. The SONG spectrometer registered the direct solar neutrons in a time interval "that nearly coincided with the Tsumeb excess shown in the figure. The later increase in the count rate of the Moscow neutron monitor at 57N/37E was due to the arrival of protons from the flare, traveling along the Parker spiral." This study by Miroshnichenko et al. (2005) is consistent with that by Kuznetsov et al. (2007) and illustrated in Figure 18, where the SONG neutron counts are for 30 s intervals.

As is clear from the above discussion, the distinct observation of solar-flare produced neutrons in terrestrial Ground Level Neutron monitors provides confirmation of proton/ and ion acceleration to several hundred MeV, because the neutrons themselves must have energies >100 MeV for a sufficient number to survive the 1-AU flight path to reach a GRL neutron monitor. Besides the 2003 October

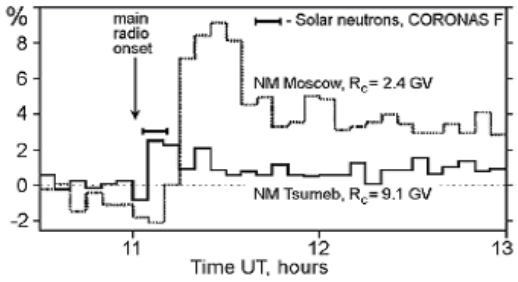

Fig. 19 Response (5 minute averages) of the Tsumeb and Moscow neutron monitors following the 2003 October 28; 4B, X17.2 solar flare. The vertical arrow indicates the start of strong radio emission at 1102 UT.The horizontal bar marks the time interval when neutrons were detected by the SONG spectrometer on the CORONAS-F spacecraft. From Miroshnichenko et al. (2005), JGR 110, A09S08. Copyright 2005 American Geophysical Union. Reproduced by permission of American Geophysical Union.

28 flare, two other large flares provided ground-level flare-neutron signals on 2003 November 2 and 4. Watanabe et al. (2005) reviewed these observations along with those of all similar events in *Solar Cycles 21 and 22*. Including *Solar Cycle 23*, there are now a total of 10 solar-neutron events observed by ground-level neutron monitors. For this set of events, the relation between the power-law spectral indices of the accelerated proton and escaping neutrons is given by:

$$\alpha_{\rm n} = (0.89 \pm 0.17) \times \alpha_{\rm p} + (0.44 \pm 0.47), \tag{1}$$

quantifying the relationship that the ion spectrum is softer than that of the neutrons. This result is based on the simulation code of Hua et al. (2002). For further considerations on this topic see Ryan (2005).

3.8 2005 January 20

The largest gamma-ray flare observed by RHESSI, occurred on 2005 January 20 in NOAA Active Region 10720 at 14N61W. In addition, it was well observed by the SONG spectrometer on CORONAS (Kuznetsov et al. 2005). The GOES time history shows the soft X-ray behavior for the event until 0800 UT as shown in Figure 20, for the the SXR channels (1–8 Å) and (0.5–4 Å). The beginning of the impulsive phase in X-rays and gamma-rays at 0642:40 UT is clearly visible (first dotted line).

The corrected count rates for several RHESSI energy channels is shown in Figure 21. Because of its higher sensitivity, the (3–6 keV) RHESSI count rate (black curve) begins before the GOES rates. The 0.8–7 MeV (orange curve) gamma-ray rate begins a slow rise at ∼0645 UT while the 7–20 MeV (green curve) began a slow increase at ∼0635 UT. This channel, the highest for RHESSI, reached a maximum just after 0645 UT.

In Figure 22, corrected count rates for the SONG spectrometer on CORONAS (Kuznetsov et al. 2005) are shown for the energy channels (0.15–0.5 MeV) and (60–200 MeV). The higher-energy gamma-rays begin a sharp increase at 0645:40 UT, about three minutes after the start of the impulsive burst of hard X-rays, indicating particle acceleration to higher energies. Figure 23 shows the energy spectra of gamma-rays for the three time intervals marked in Figure 22.

Figure 23 shows that there are significant differences in the spectra for the three time intervals I, II and III. In particular, there is a sharp increase in flux in time interval II with a significant flattening of the spectrum as shown in the middle spectrum. Kuznetsov et al. (2005) attributed this as to π^0-decay gamma-rays that have a broad peak centered at 67.5 MeV.

Comparing the SONG fluxes above 100 MeV for the 2003 October 28 to that of the 2005 January 20 flare suggests that relativistic neutrons from the later flare may also reach the Earth. Although the subsolar point hovered over the longitude of the Tibet Yangbajing Neutron monitor (YBJB NM) during this

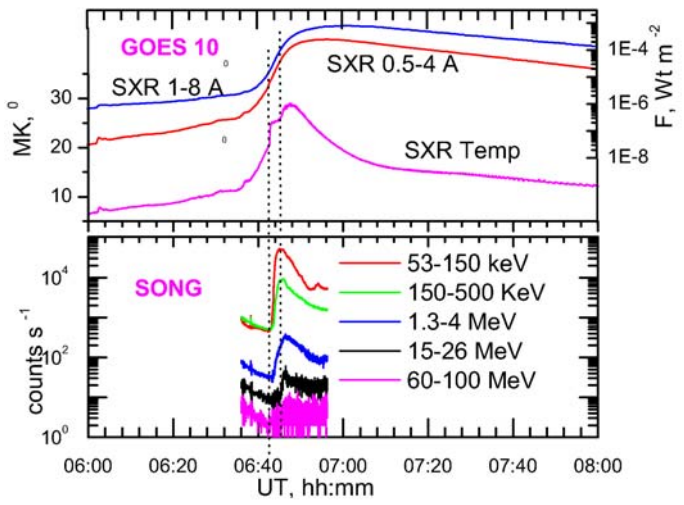

Fig. 20 Upper panel: Soft X-ray measurement by GOES on 20 January. Lower panel: Excess in hard X-ray and gamma-ray channels observed by SONG on CORONAS-F (From Kuznetsov et al. 2005, in Proc. 29th Int. Cosmic Ray Conf., Pune 2005, Vol. 1, pp 49–52, Eds. B. S. Acharya et al., Publ. TIFR, Mumbai, India 2005).

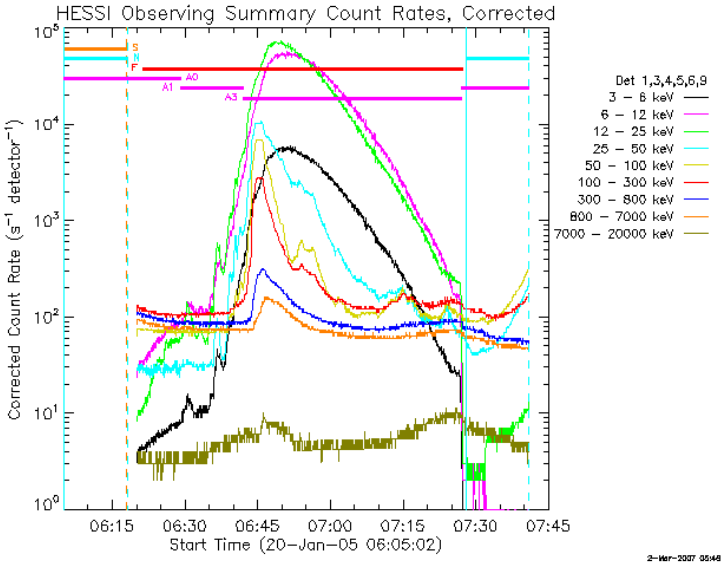

Fig. 21 The corrected count rates for several RHESSI energy channels. From the Quicklook Browser in the RHESSI Data And Software Center at *http://hesperia.gsfc.nasa.gov/rhessidatacenter/.*

flare, it was well south of the instrument with a zenith angle of 51°. Miyasaka et al. (2005) have made an extensive study of the ground-level enhancement (GLE) observed by the YBJB NM that started at 0649 UT and reached a 2% intensity maximum at 0705 UT. Because the SONG high energy signal began at 0645:40 UT, and is presumed to be meson-decay gamma-rays, one should expect a flux of neutrons at

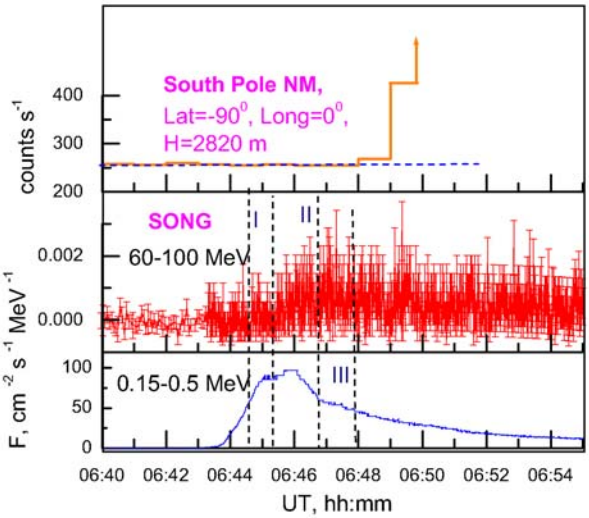

Fig. 22 The temporal profile of measurements at two γ-ray channels of SONG along with the onset of GLE observed by the South Pole NM. From Kuznetsov et al. (2005), in Proc. 29th Int. Cosmic Ray Conf., Pune 2005, Vol. 1, pp.49–52, Eds. B. S. Acharya et al., Publ. TIFR, Mumbai, India (2005).

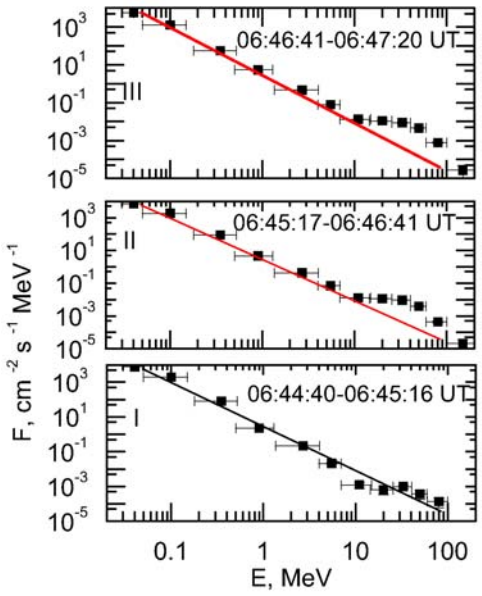

Fig. 23 The energy spectra of γ-rays observed by SONG during the three time intervals marked in Figure 22. Note that the lower spectrum is for I, the middle for II, and top for III. From Kuznetsov et al. 2005, in Proc. 29th Int. Cosmic Ray Conf., Pune 2005, Vol. 1, pp.49–52, Eds. B. S. Acharya et al., Publ. TIFR, Mumbai, India (2005).

the Earth (see above). Relativistic neutrons ($\nu \sim c$) could have been produced just after the start of the sharp increase at 0645:40 UT of the (60–200 MeV) gamma-rays. These neutrons should have arrived at 0646 with the bulk of the neutrons at lower energies arriving several minutes later.

Using the Monte Carlo code of Clem & Dorman (2000), Miyasaka et al. (2005) estimated the YBJ NM yield function, and with the neutron spectrum of the 2003 October 28 flare (Bieber et al. 2005), predicted an expected YBJ NM signal. This result is shown in Figure 24. Miyasaka et al. (2005) also reported that the YBT neutron telescope (Katayose et al. 1999) located in the same vicinity as the YBJ NM did not observe neutrons during the period indicated in red in Figure 24.

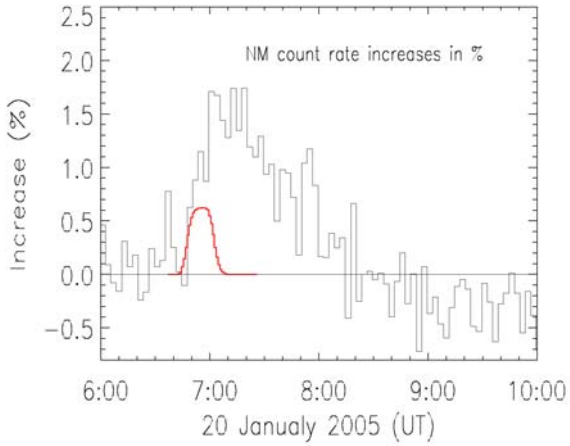

Fig. 24 The YBJ NM 3 minute average intensity. The red curve is the expected intensity increase assuming the existence of a solar neutron onset at 6:36 ST = 6:44.3 UT. From Miyasaka et al. (2005), in Proc. 29th Int. Cosmic Ray Conf., Pune 2005, Vol. 1, pp 241–244, Eds. B. S. Acharya et al., Publ. TIFR, Mumbai, India (2005).

4 SOME PROPOSED ACCELERATION MECHANISMS

Among the many interesting aspects of this phenomena are the mechanisms capable of accelerating ions and/or electrons to GeV energies. The fundamental ingredient for accelerating a charged particle is an electric field (see Jokipii 1979). The electric field can arise in a variety of ways and they have been studied by several researchers. In general, the change in the kinetic energy, ΔT, of a charged particle, q, in a macroscopic electric field $\boldsymbol{E}(\boldsymbol{r},t)$ in a plasma can be expressed as:

$$\Delta T = q \int_0^{\Delta t} dt\, \boldsymbol{E} \cdot \boldsymbol{W} \tag{2}$$

where $\boldsymbol{W}$ is the particle velocity. We note that the position of the charge, $\mathbf{r}(t)$, defines its instantaneous trajectory so that the propagation geometry is intimately connected to the particle's acceleration! The complexity of the problem is immediately evident.

Aschwanden (2002) has reviewed recent work on the particle acceleration problem. In Figure 25 we show a schematic diagram from Aschwanden (2002) illustrating how the accelerated particles are related to the observations. The five steps in flare dynamics and kinematics considered by Aschwanden (1998) are:

(1) Particle acceleration.
(2) Particle injection onto a magnetic field line and escape from the acceleration region.

(3a) Free-streaming particle propagation or transport.
(3b) Particle mirroring in a trap (plus precipitation or not).
(4) Energy loss by radiation.

Steps (3a) and (3b) occur in parallel, so there is generally a bifurcation in the particle path, with some particles propagating directly to the energy loss site, while other particles are stored in a trap and mirror many times (emitting gyrosynchrotron radiation if electrons), before losing their energy or escaping by precipitation and propagating to their final energy loss site. These five conceptual steps are illustrated in Figure 25. Each of these processes has its own energy-independent timing which must be included in any model describing the hard X-ray/gamma-ray and microwave/sub-mm spectra. Therefore, any proposed acceleration process cannot be realistically tested against the observations unless the propagation or transport effects are taken into account.

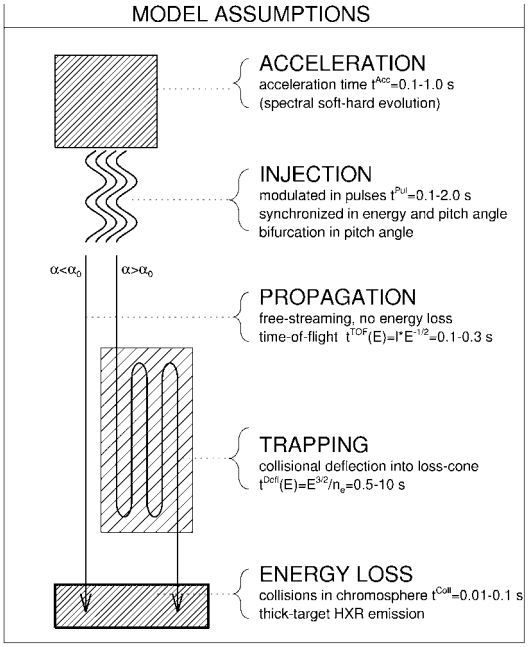

Fig. 25 A schematic diagram from Aschwanden (2002) illustrating how the accelerated particles are related to the observations. From Aschwanden (2002), Space Science Reviews 101, 1–227, Figure 63, p105. With kind permission from Springer Science and Business Media.

A few key characteristics set the acceleration process of our particular events apart from that of numerous impulsive gamma-ray flares, where the emission rises quickly and extends over only a few minutes. The problem in that case is how to accelerate the ions to 10 MeV so quickly. The problem is different here. The energies first extend to much higher values, energies that we normally associate with Ground Level Event (GLE) particles. The onset of this radiation is often delayed by several minutes from the impulsive part of the flare and, lastly, it can extend for hours, measurable with sensitive instruments. The prolonged nature of the emission also seems devoid of temporal structure, but this is only measurable in the few cases where the instantaneous intensity is great enough. With these objectives, we briefly review a few attempts to model the observations.

We observe the following, and in an attempt to reach general conclusions about a class of Solar Flares, apply these observations and their attendant restrictions to the entire class and critically ask the

question if such a generalization works. We first note that the emission is largely, if not entirely, of ion origin. The identical behavior of the 2.223 MeV line and the high energy emissions of the 9, 11 and 15 June 1991 events support this (Rank et al. 2001). Secondly, the absence of fine temporal structure points toward the process taking place over very large volumes where such fine detail is averaged over the dynamics of the entire volume, resulting in a smooth evolution of the emission. Lastly, the prolonged emission virtually precludes *passive* trapping of the ions in a coronal loop. With emission extending for 10^4 s, the mean free path for particle scattering in a magnetic field is 20 AU. This is unlikely on two fronts, the first being that a large flare has taken place in the vicinity imparting 10^{32} erg of mechanical energy to the corona. In addition, the value of δB/B to achieve such a long path length is of order 0.05 for 1 GeV protons (without taking into account drift losses), far quieter than the solar wind itself of order unity (from GLE anisotropy measurements). Thus, by the process of elimination, we fall back on a picture of prolonged acceleration in a large volume where transport effects govern the overall exponential decay of the emission. The onset and delay can be understood by noting that only when a sufficient number of ions exceed the pion production threshold will the high-energy gamma-ray emission begin. Thus, the acceleration can begin before the onset of the high-energy phase, but this only becomes visible once ions exceed the pion threshold.

Four basic processes are candidates: (1) second-order Fermi acceleration in a large magnetic trap, (2) betatron acceleration, (3) statistically coherent electric fields over a large current sheet and (4) downstream diffusion of ions from a large coronal (and eventually interplanetary) shock (first order Fermi acceleration) onto the solar surface. All four have their strengths but suffer weaknesses too.

4.1 Diffusion Models (Stochastic-Second Order Fermi)

A relatively early model to explain the observations of the 1982 June 3 was studied by Ryan & Lee (1991) in which they assumed a flaring turbulent MHD wave field in a coronal loop, connected to the photosphere, and containing a uniform thermal plasma. The turbulence causes diffusion of the particles in physical and momentum space. Using this model, applied to the parameters of the 1982 June 3 observations, good agreement was obtained between the predicted and observed time histories for an assumed loop length of 10^5 km and a spatial diffusion time of 100–450 s. This model is essentially a single stage model in which the injected particles lead to both the nuclear line emission and the later pion production.

The first attempt to model the 1982 June 3 flare observations was made by Murphy, Dermer & Ramaty (1987) who assumed two particle populations to explain the initial gamma-ray emission and the later pion decay gamma-ray emission. Later Mandzhavidze & Ramaty (1992), in studying the pion decay emissions, included the production of gamma-rays from the decay of charged pions, and the effects of particle trapping and pitch angle scattering of the particles. By varying the scattering properties of particles in the loop, it was found possible that a single phase acceleration could be made consistent with the 1982 June 3 flare observations and the linear dimension of the loop.

However, because the time scales are so great, the particles must continuously be accelerated by the same scattering process by second-order Fermi acceleration, so that the time scales for spatial diffusion and momentum diffusion are inextricably linked. The spatial diffusion time in a large linear structure with loss boundaries at the end points is given by $l^2/\pi^2\kappa$, where l is the loop length and κ is the spatial diffusion coefficient. This time scale is linked to the acceleration time scale by the same scattering process that determines κ. The greater κ is, the less momentum diffusion (acceleration) will occur. Without visual measurements of the linear trap (loop), many possibilities for l and κ exist that conform to the high-energy phenomenon. Ryan & Lee (1991) fit the 1982 June 3 data to a variety of l and κ values. The loop length in all cases was long, e.g., of order 10^5 km or greater so as to provide sufficient time for acceleration to occur before the particles were lost to precipitation. Not included in their model was the means to capture or maintain the turbulence for this length of time or losses from particle drifts in the curved and inhomogeneous magnetic field.

As pointed out in Section 2, when pions are produced, their decay gamma-ray spectrum depends sensitively on the accelerated proton spectra, and this point also applies to the following discussion!

4.2 Betatron Accleration (Magnetic Trap)

Bogachev & Somov (2005) studied First-order Fermi and Betatron acceleration in a collapsing magnetic trap which results after reconnection at a 3D null point. Brown & Hoyng (1975) also suggested this process to explain the intense electron bremsstrahlung in the 1972 August 4 solar flare. Basically, the induced electric field arises from Faraday's Law where the collapsing magnetic field and the first adiabatic invariant results in energy being imparted to the gyrating particle (see also Aschwanden 2002). This model is appropriate for electron acceleration of a few hundred keV. Ions with their greater momentum and gyroradius would not stay confined to the trap.

4.3 Coherent Electric Fields (Reconnection Models)

The discovery of accelerated electrons up to 300 keV in the terrestrial magnetotail, observed by the Wind spacecraft, has been explained by magnetic reconnection (Øieroset et al. 2002). Currently, the electric fields produced by reconnection of coronal magnetic fields is a promising mechanism for the acceleration of the high energy ions and electrons in solar flares. Indeed, Priest & Forbes (2000) have stressed the importance of magnetic reconnection in space plasmas. We focus on how reconnection can provide the high energy ions and electrons of interest here.

A recent study by Litvinenko (2006) provided a promising approach to a solution of this problem. Litvinenko (2006) showed that proton and electron acceleration, associated with "fan magnetic reconnection" can accelerate protons to an energy "of the order of a few MeV" and accelerate electrons to energies "of a few hundred keV" in the case of classical electric resistivity. For turbulent resistivity, ion energies "up to a few hundred MeV can be reached." The calculations were done for the electric and magnetic fields in the vicinity of magnetic nulls as defined by Priest & Titov (1996) where "spine curves" and "fan surfaces" are defined. See also publications by Craig & Henton (1995), Craig & Fabling (1996) and Heerikhuisen & Craig (2004). Litvinenko (2006) concluded that "fan reconnection" rather than "spine reconnection" can provide the large energy release rates necessary for large coronal flares. He also suggested that spine reconnection may not be an effective energy release mechanism for a solar flare, based on an analysis by Craig & Watson (2000). Of course, the results of such calculations must be combined with appropriate transport effects to explain (model) the observations of a suitable flare as discussed by Aschwanden (1998). Furthermore, to explain an event like the 1991 June 11 flare, the acceleration process must last for several hours, unless long term storage occurs as proposed by Kanbach et al. (1993).

4.4 Shock Acceleration (First order Fermi)

Shocks are a demonstrated accelerator of particles. This can be seen in the Earth's environment and in distant radio galaxies as well as in interplanetary space. It is not known if they play a role in flares, *per se.* Two possibilities exist for accelerating flare particles in shocks. These are blast waves and standing slow shocks around the reconnection region. The standing slow shocks around the reconnection region enjoy the advantage of time for particle acceleration. The propagating blast wave must work fast to accelerate particles, before it loses its strength. Work on the blast-wave problems was pursued by Lee & Ryan (1986) who modeled a coronal blast wave acceleration of ions. On the time scale of a few seconds, MeV ions were produced from injection ions of $\sim$100 keV. With the speed of a blast wave, acceleration within the corona is limited by the travel time of the shock, i.e., tens of seconds. Although additional acceleration can take place well away from the flare region, transporting those particles back to the lower corona becomes increasingly difficult.

A more promising possibility is that protons and ions accelerated by interplanetary shock waves produced by a coronal mass ejection diffuse back toward the Sun, against the fluid flow, to precipitate onto the solar surface. We know of no quantitative work on this prospect. However, Kahler & Ragot (2008) considered the interaction of GLE protons and ions with the ambient solar wind. They find that it

is possible to produce the pion-decay photon luminosity from the 1991 June events, although how these remote interactions produce the neutron-proton capture line remains a problem.

We wish to emphasize that solar-flare particle acceleration cannot be understood unless the problem of production of ions and electrons to GeV energies is *solved!* This requires confronting any theoretical model with multiwavength observations of several flares.

4.5 The Pion Decay Spectrum

In interpreting the high energy emissions in the 1982 June 3 event, several different accelerating mechanisms have been suggested, all of which explain the observations; e.g., Murphy, Dermer & Ramaty (1987), Ryan & Lee (1991) and Mandzhavidze & Ramaty (1992). This conundrum inspired Alexander and MacKinnon (1993) to focus on the proton spectral shape above the pion-production threshold (PPT). Their essential point was that the shape of the proton spectrum above the PPT determines the shape (width) of the pion peak, centered at 67.5 MeV and extending to several hundred MeV. Of additional significance is the production of the bremsstrahlung spectrum from electrons resulting from the decay of $\pi^{\pm}$ mesons (see Manzhavidze & Ramaty 1992). Several events also indicate a steep photon spectrum that could be due to bremsstrahlung from primary accelerated electrons. Therefore, the question is: How to determine the acceleration mechanisms(s) from observing the gamma-ray spectrum above $\sim$50 MeV? This cannot be done without multiwavelength observations of several flares so that all feasible mechanisms and models can be evaluated.

The High-Energy Meson-producing Flares discussed in this paper appear to be similar, if not the same, as the Long-Duration Gamma-Ray Flares discussed by Ryan (2000). They are both characterized by an initial impulsive phase with hard X-ray/gamma-ray emission to $\sim$10 MeV followed by a time extended phase with evidence for $>$50 MeV pion decay gamma-ray emission and electron bremsstrahlung approaching, and maybe surpassing, one-hundred MeV, followed sometimes by the detection of ground-level neutrons. Basically, the extended phase is characterized by a much harder photon spectrum than that of the impulsive phase.

The emerging picture is that acceleration of the highest energy ions takes time—considerable time, as compared to the duration of the impulsive phase. A telling counterexample is that of the 1980 June 21 flare shown in panel (a) of Figure 3. This was only an impulsive phase flare, and although it achieved high-energy gamma-ray and neutron production, we can only infer the production of π mesons. With more time, higher energies may have been produced allowing us to classify it as a meson-producing flare. Gan & Rieger (1999) identified cutoff energies in the energetic ion spectrum that is a result of a truncated acceleration process. As a result of the prolonged acceleration of these particles, the transport of these ions is a factor to be considered, where the volume of the corona taking part in this process must be correspondingly large, approaching one solar radius in one or all dimensions. If this volume is not sufficiently large, the acceleration process has limited time to operate before the ions are lost. The other aspect that we note is that even for dimensions of one solar radius, the ions will be lost by drifts or scattering because the transit time for these particles over one solar radius is of order 1 s. These observations drive us to conclude that the large affected volume of the corona is either extraordinarily MHD quiet so that mirroring is efficient or it is very MHD noisy with the associated turbulence constraining the escape of the particles. We prefer the latter explanation because the MHD turbulence is also effective in accelerating the ions to high energies over long periods of time, precisely the phenomenon we wish we understand. Our many observations of this phenomenon suggest that the energy gains are slow, the particle transport is slow and inefficient, the energy density of the acceleration volume is low and the transport of the ions constraining the particles must also drive the precipitation of the particle to the low corona, where they can produce mesons and emit radiation.

As a corollary, intense X-ray or gamma-ray flares exhibiting no extended phase should not be expected to exhibit significant meson-related emission. This may be a result of mostly open field lines above the flare, producing a low altitude free-escape boundary for the energetic ions or the lack of an energy source that the ions can tap, such as the charge separation of a large scale electric field or an intense MHD turbulence field.

5 THE FERMI GAMMA RAY SPACE TELESCOPE (GLAST) MISSION

The primary mission of the Gamma Ray Large Area Space Telescope (GLAST), which was launched on 2008 June 12, is to study the celestial gamma-ray emissions above 30 MeV to several-hundred GeV, with the LAT (Large Area Telescope). The GBM (Gamma-Ray Burst Monitor) detects photon bursts from 10 keV to 25 MeV. The LAT is an imaging telescope with a wide field of view in a circular orbit of 550 km altitude. Therefore, the Sun will be its field of view for a large fraction of the sunlight phase of the orbit.

At *"The FIRST GLAST SYMPOSIUM*" at Stanford, CA on 2007 February 6–8, Share & Murphy (2007) reviewed the prospects for high-energy solar-flare gamma-ray observations during Solar Cycle 24 by GLAST. The observations can be correlated with high-resolution imaging/spectroscopy by RHESSI from $\sim$1 keV to 16 MeV and other space observatories such as ACE, TRACE, SOHO, HINODE and STEREO and various ground-based observatories covering electromagnetic and particle radiations. It is expected that the LAT will normally have more than 20% solar exposure and up to $\sim$60% exposure during a ToO (Target of Opportunity) period. The ToO can permit long term observation of a promising active region greatly increasing the chance of a new and telling observation. The possible electromagnetic emissions that may be observed from energetic flares are described in Section 2 of this paper.

As we have discussed in Section 3, many high-energy flares also have associated high-energy neutrons that can be detected by Earth-orbiting detectors or even by ground-level neutron monitors and neutron telescopes (Muraki et al. 1993). The prospect that LAT could detect neutrons produced in a solar flare was also discussed at "The FIRST GLAST SYMPOSIUM" by Murphy & Dermer (2007) and by Longo et al. (2007). Preliminary model calculations, using estimates by Hua et al. (2002), indicate that about 1% of the neutrons passing through the LAT would produce a trigger and be recorded. Furthermore, analysis of the LAT contribution to the actual solar-flare gamma-ray spectrum, can be an independent measure of an actual flux.

With high enough gamma-ray energies, *Fermi* may be able to discriminate between one or more point-like radiation patterns on the disk as opposed to a diffuse bright area responsible for the gamma emission. Such a discrimination may help resolve whether the energetic ions are trapped in a magnetic loop or are precipitating diffusely from a receding coronal shock. However, even with the large collecting area of *Fermi*, such an observation will be rare, because it requires considerable gamma-ray intensity above 1 GeV where the instrument resolution is good enough to make such a telling observation.

6 FUTURE MISSIONS TO MEASURE ENERGETIC FLARE PARTICLES

A full understanding of the acceleration processes leading to the highest energy ions and electrons requires multiwavelength observations of several suitable flares. Specifically, this means making high resolution imaging and spectral observations from the infrared to several hundred MeV. In addition, the determination of the energy spectrum of neutrons both in the instrument complex and by ground based neutron spectrometers provides complementary information on the high energy flare. We envision space based platforms as well as a Lunar base. Also, observations by suitable instruments on a solar orbiter will add additional insights.

6.1 Earth Orbit

Currently, France and China have proposed SMESE (Small Explorer for Solar Eruptions) which is a microsatellite flare mission with instruments covering the range from the infrared and ultraviolet to 600 MeV gamma rays. If approved and funded by both countries, the satellite could be in orbit during the declining phase of Solar Cycle 24 in 2013 or later. Recently Vial et al. (2008) gave a detailed description of the planned instrument complex, which includes:

LYOT (LYman alpha imaging Orbiting Telescope), HEBS-X and HEBS-gamma (High Energy Burst Spectrometers) covering the X-ray and gamma-ray energy range from 10 keV to 600 MeV and DESIR (DEtection of Solar Infrared Radiation).

LYOT is a Lyman α coronagraph and includes a disk imager with a high cadence (10 s) and with high sensitivity. The coronagraph has the ability to measure the polarization of the radiation, allowing an estimate of the coronal magnetic field. DESIR gives a low spatial resolution image, and measures the flux density in two windows at 35–80 μm and 100–250 μm. This instrument will be able to determine an approximate localization of far-infrared emitting sources (FIR), which are not understood (see Kaufmann 2004).

The HEBS uses three $LaBr_3$ scintillators to cover three energy bands: 10–500 keV with 1 s time resolution, 0.3–9 MeV with 1 s time resolution and 5–600 MeV with 4 s time resolution. The time resolutions given are for the *watching mode* and time resolutions down to 32 ms are possible in the *event mode.* The planned altitude is in the range of 650–750 km, to have a long orbital lifetime and to avoid too great a radiation belt exposure. The Satellite Control Center will be at CNES in Toulouse.

6.2 Lunar Based

The Exploration initiative will certainly stimulate proposals for solar flare observations from the Moon. In fact, since the successful Apollo missions, there have been numerous workshops on this subject. As an example, in 1990, a workshop was held in Annapolis, MD on Astrophysics from the Moon. One paper by Peterson (1990) describes *Hard X-ray and High-Energy Gamma-Ray imaging telescopes* appropriate for Solar flare observations. Table 3 summarizes the properties of the candidate instruments. The High-Energy telescope consists of a spark chamber array patterned after the Energetic Gamma Ray Experiment Telescope (EGRET) on the CGRO. The high spatial resolution is achieved by use of a coded aperture mask. However, the high energy X-ray and gamma-ray background from the intense primary cosmic-ray flux presents a major challenge to design a suitable Solar Observatory (see also Davis et al. 1990 and Hudson 1990).

Table 3 Modular Imaging Photon Spectrometer Instrument Parameters

Hard X-ray/Medium Energy Gamma-Ray Telescope	
Energy Range:	10 keV to 20 MeV
Spectral Resolution:	$E/\Delta E \sim 500$ @ 1 MeV
Spatial Resolution:	1–10 arcsec (max)
Narrow Line Sensitivity:	3×10^{-7} ph cm^{-2} s^{-1}
Dimensions:	~ 5 m^3
Weight:	2000 kg
Data Rate:	50 kbps
Power:	1.5 KW
High-Energy Gamma-Ray Telescope	
Energy Range:	20 MeV to 50 GeV
Spectral Resolution:	$E/\Delta E \sim 25$
Spatial Resolution:	1–10 arcsec (max)
Integral Continuum Sensitivity:	10^{-9}ph cm^{-2}s^{-1}
Dimensions:	5 m^3
Weight:	5000 kg
Data Rage:	35 kbps
Power:	1.5 KW

6.3 Deep Space Missions

Three deep space missions are in different states of study or preparation. These are the Solar Orbiter mission of ESA and for NASA, Solar Sentinels and Solar Probe. All these missions will possess, in one form or another, gamma-ray and neutron detectors or spectrometers. All these missions have been conceived to get much closer to the Sun than 1 AU, with Solar Probe having several passes within

about 10 solar radii. Besides enjoying the r^2 advantage, this proximity will allow measurement of low-energy neutrons, i.e., below 10 MeV. These are neutrons that do not survive the trip to 1 AU. Such low-energy neutron measurements will shed light on the "invisible" energetic proton spectrum below a few MeV and the composition of the particles producing the neutrons. An ion population enhanced in heavy ions will be more prolific in neutron production than for the same gamma-ray emission. When these low-energy neutrons are emitted is also a question. Do they emerge before the impulsive phase as a precursor, during the impulsive phase, or do they preferentially emerge when the higher energy neutrons seem to dominate? Only by getting close to the Sun for these measurements will we know. To make such measurements, good energy measurements of individual neutrons will likely be necessary to remove the effect of velocity dispersion.

In conclusion, we want to emphasize again that understanding the mechanisms which accelerate particles (ions and electrons) to GeV energies in solar flares is crucial to the flare problem, *per se*!

Acknowledgements The authors wish to thank the referee for constructive suggestions which improved the paper.

Appendix A: LONG DURATION GAMMA-RAY FLARES

Table A.1 Long Duration Gamma-ray Flares

Year	Month	Day	Duration (s)	τ1 (min)	τ2 (min)	Ref.
1982	6	3	1200	1.15±0.14	11.7±3.0	1, 2
1984	4	24	900	3.23±0.07	≥10	2
1988	12	16	600	3.34±0.30		2
1989	3	6	1500	2.66±0.27		2
1989	9	29	>600			3
1990	4	15	1800			5
1990	5	24	500	0.35±0.02	22±2	4, 5, 6
1991	3	26	600			7, 8
1991	6	4	10000	7±0.8	27±7	9, 10
1991	6	6	1000			9
1991	6	9	900			9, 11
1991	6	11	30000	9.4±1.3	220±50	9, 12, 13
1991	6	15	5000	12.6±3.0	180±100	7, 8, 12

[1]Chupp (1990); [2]Dunphy and Chupp (1994); [3]Vestrand and Forrest (1993); [4]Debrunner et al. (1997); [5]Trotter (1994); [6]Debrunner et al. (1998); [7]Akimov et al. (1991); [8] Akimov et al. (1994c); [9]Schneid et al. (1996); [10]Murphy et al. (1997); [11]Ryan et al. (1994a); [12]Rank et al. (1996); [13]Kanbach et al. (1993)

References

Alexander, D., & MacKinnon, A. L. 1993, Advances in Space Research, 13, 259
Akimov, V. V., et al. 1991, in Proc. 22th Int. Cosmic Ray Conf. (Dublin), 3, 73
Akimov, V. V., Leikov, N. G., Belov, A. V., et al. 1994, in AIP Conf. Proc. 294, High-energy solar phenomena, eds. Ryan, J. M., & Vestrand, W., T., 106
Akimov, V. V., et al. 1996, Sol. Phys., 166, 107
Aschwanden, M. J. 1998, ApJ, 502, 455
Aschwanden, M. J. 2002, Space Science Reviews, 101, 1
Bieber, J. W., Clem, J., Evenson, P., Pyle, R., Ruffolo, D., & Sáiz, A. 2005, Geophys. Res. Lett., 32, 3
Bogachev, S. A., & Somov, B. V. 2005, Astronomy Letters, 31, 537
Brown, J. C., & Hoyng, P. 1975, ApJ, 200, 734

Chupp, E. L., Forrest, D. J., Higbie, P. R., Suri, A. N., Tsai, C., & Dunphy, P. P. 1973, Nature, 241, 333
Chupp, E. L., et al. 1982, ApJ, 263, L95
Chupp, E. L., et al. 1987, ApJ, 318, 913
Chupp, E. L. 1990, ApJS, 73, 213
Clem, J. M., & Dorman, L. I. 2000, Space Science Reviews, 93, 335
Craig, I. J. D., & Henton, S. M. 1995, ApJ, 450, 280
Craig, I. J. D., & Fabling, R. B. 1996, ApJ, 462, 969
Craig, I. J. D., & Watson, P. G. 2000, Sol. Phys., 194, 251
Davis, J. M., Balasubramaniam, K. S., Gary, G. A., & Moore, R. L. 1990, in AIP Conf. Proc. 207, Astrophysics from the Moon (New York: AIP), 567
Debrunner, H., Lockwood, J. A., & Ryan, J. M. 1993, ApJ, 409, 822
Debrunner, H., et al. 1997, ApJ, 479, 997
Dunphy, P. P., & Chupp, E. L. 1991, in Proc. 22th Int. Cosmic Ray Conf. (Dublin), 3, 65
Dunphy, P. P., Chupp, E. L., Bertsch, D. L., Schneid, E. J., Gottesman, S. R., & Kanbach, G. 1999, Sol. Phys., 187, 45
Evenson, P., Meyer, P., & Pyle, K. R. 1983, ApJ, 274, 875
Forrest, D. J., Vestrand, W. T., Chupp, E. L., Rieger, E., Cooper, J. F., & Share, G. H. 1985, in Proc. 19th Int. Cosmic Ray Conf, 4, 146
Gan, W. Q., & Rieger, E. 1999, Sol. Phys., 186, 311
Halprin, A., Andersen, C. M., & Primakoff, H. 1966, Physical Review , 152, 1295
Heerikhuisen, J., & Craig, I. J. D. 2004, Sol. Phys., 222, 95
Heyvaerts, J., Priest, E. R., & Rust, D. M. 1977, ApJ, 216, 123
Hua, X.-M., Kozlovsky, B., Lingenfelter, R. E., Ramaty, R., & Stupp, A. 2002, ApJS, 140, 563
Hua, X.-M. & Lingenfelter, R. E. 1987, Sol. Phys., 107, 351
Hudson, H. 1990, in AIP Conf. Proc. 207, Astrophysics from the Moon (New York: AIP), 109
Hurford, G. J., Krucker, S., Lin, R. P., Schwartz, R. A., Share, G. H., & Smith, D. M. 2006, ApJ, 644, L93
Jokipii, J. R. 1979, in AIP Conf. Proc. 56, Particle Acceleration Mechanisms in Astrophysics (La Jolla: AIP), 1
Kahler, S. W., & Ragot, B. R. 2008, ApJ, 675, 846
Kanbach, G., et al. 1993, A&AS, 97, 349
Katayose, Y. 1999, In Proc. 26th Int. Cosmic Ray Conf. (Salt Lake City), eds. D. Kieda, M. Salamon, and B. Dingus, 6, 58
Kaufmann, P., et al. 2004, ApJ, 603, L121
Kiener, J., Gros, M., Tatischeff, V., & Weidenspointner, G. 2006, A&A, 445, 725
Kocharov, L. G., Lee, J. W., Zirin, H., Kovaltsov, G. A., Usoskin, I. G., Pyle, K. R., Shea, M. A., & Smart, D. F. 1994a, Sol. Phys., 155, 149
Kocharov, L. G., et al. 1994, Sol. Phys., 150, 267
Kocharov, L., et al. 1998, A&A, 340, 257
Koval'tsov, G. A., Kocharov, G. E., Kocharov, L. G., & Usoskin, I. G. 1994, Astronomy Letters, 20, 658
Kuznetsov, S. N., & et al. 2005, in Proc. 29th Int. Cosmic Ray Conf. (Pune), eds. Sripathi Acharya, Sunil Gupta, P. Jagadeesan, Atul Jain, S. Karthikeyan, Samuel Morris, & Suresh Tonwar, 1, 49
Kuznetsov, S. N., Kurt, V. G., Yushkov, B. Y., Myagkova, I. N., Kudela, K., Kaššovicová, J., & Slivka, M. 2006, in Contributions of the Astronomical Observatory Skalnate Pleso, 36, 85
Lee, M. A., & Ryan, J. M. 1986, ApJ, 303, 829
Lin, R. P. 2006, Space Science Reviews, 124, 233
Lingenfelter, R. E., & Ramaty, R. 1967, High-Energy Nuclear Reactions in Astrophysics, ed., B. S. P Shen (Benjamin: New York), 99
Litvinenko, Y. E. 2006, A&A, 452, 1069
Longo, F. 2007, in AIP Conf. Proc. 921, The First GLAST Symposium, 466
Mandzhavidze, N., & Ramaty, R. 1992, ApJ, 389, 739
Marschhäuser, H., Rieger, E., & Kanbach, G. 1994, in AIP Conf. Proc. 294, High-Energy Solar Phenomena - a New Era of Spacecraft Measurements, eds. J. Ryan and W. T. Vestrand (New York: AIP), 171

McConnell, M., Bennett, K., Forrest, D., Hanlon, L., Ryan, J., Schönfelder, V., Swanenburg, B. N., & Winkler, C. 1993, Advances in Space Research, 13, 245
Miroshnichenko, L. I., Klein, K.-L., Trottet, G., Lantos, P., Vashenyuk, E. V., Balabin, Y. V., & Gvozdevsky, B. B. 2005, Journal of Geophysical Research, 110, A09S08
Miyasaka, H., & et al. 2005, in Proc. 29th Int. Cosmic Ray Conf. (Puna), 1, 241
Morrison, P., 1958, Nuovo Cimento, 7, 858
Muraki, Y., Takahashi, T., & et al. 1993, in Proc. 23rd Int. Cosmic Ray Conf. (Calgary), 3, 171
Murphy, R. J., Dermer, C. D., & Ramaty, R. 1987, ApJS, 63, 721
Murphy, R. J., & Share, G. H. 2000, in AIP Conf. Proc. 510, The Fifth Compton Symposium, eds. M. L. McConnell and J. M. Ryan, 559
Murphy, R. J., & Dermer, C. D. 2007, in AIP Conf. Proc. 921, The First GLAST Symposium, eds. S. Ritz, P. Michelson, and C. Meegan, 468
Øieroset, M., Lin, R. P., Phan, T. D., Larson, D. E., & Bale, S. D. 2002, Physical Review Letters, 89, 195001
Peterson, L. E. 1990, in AIP Conf. Proc. 207, Astrophysics from the Moon (New York: AIP), 345
Priest, E. R., and Titov, V. S., 1996, Phil. Trans. Roy. Soc. London A, 354, 2951
Priest, E., & Forbes, T. 2000, Magnetic Reconnection: MHD theory and applications (Cambridge: Cambridge Univ. Press)
Primakoff, H. 1951, Physical Review , 81, 899
Ramaty, R., Hua, X.-M., Kozlovsky, B., Mandzhavidze, N., & Lingenfelter, R. E. 1992, in Compton Observatory Science Workshop, ed. C. Shrader et al. (Washington: NASA), 480
Ramaty, R., & Mandzhavidze, N. 1994, in AIP Conf. Proc. 294, High-Energy Solar Phenomena - a New Era of Spacecraft Measurements, eds. J. Ryan and W. T. Vestrand (New York: AIP), 26
Rank, G., 1996, PhD Thesis, Techn. Univ. Munich
Rank, G., et al. 1996, in AIP Conf. Proc. 374, High Energy Solar Physics, eds. Reuven Ramaty, Natalie Mandzhavidze, and Xin-Min Hua (New York: AIP), 219
Rank, G., Ryan, J., Debrunner, H., McConnell, M., & Schönfelder, V. 2001, A&A, 378, 1046
Rieger, E. 1994, ApJS, 90, 645
Rieger, E. 1998, Sol. Phys., 180, 473
Rieger, E., Gan, W. Q., & Marschhäuser, H. 1998, Sol. Phys., 183, 123
Rieger, E., & Marschhauser, H. 1990, in MAX '91 Workshop 3, ed. R. Winglee, & A. Kiplinger (Boulder: Univ. Colorado), 68
Rieger, E., Treumann, R. A., & Karlický, M. 1999, Sol. Phys., 187, 59
Ryan, J. M., & Lee, M. A. 1991, ApJ, 368, 316
Ryan, J., et al. 1993, in AIP Conf. Proc 280, eds. Friedlander, M., Gehrels, N., and Macomb, D. J. (New York: AIP), 631
Ryan, J. M. 2000, Space Science Reviews, 93, 581
Ryan, J. M. 2005, in Proc. 29th Int. Cosmic Ray Conf. (Puna), 10, 357
Share, G. H., & Murphy R. J. 1999, in 26th Int. Cosmic Ray Conf., eds. D. Kieda, M. Salamon, and B. Dingus (Salt Lake City), 6, 13
Share, G. H., & Murphy R. J. 2000, in ASP Conf. Ser. 206, High Energy Solar Physics-Anticipating HESSI, ed. R. Ramaty and N. Mandzhavidze (San Francisco: ASP), 377
Share, G. H., & Murphy, R. J. 2006, in AGU Geophysical Monograph Series, eds. N. Gopalswamy, R. Mewaldt, J. Torst, 165, 177
Share, G. H., & Murphy, R. J. 2007, in AIP Conf. Proc. 921, The First GLAST Symposium, 109
Trottet, G., Vilmer, N., Barat, C., & et al. 1993, A&AS, 97, 337
Vial, J.-C., et al. 2008, Advances in Space Research, 41, 183
Vestrand, W. T., Share, G. H., Murphy, R. J., & et al. 1999, ApJS, 120, 409
Vilmer, N., MacKinnon, A. L., Trottet, G., & Barat, C. 2003, A&A, 412, 865
Watanabe, K., et al. 2005, in Proc. 29th Int. Cosmic Ray Conf. (Puna), 1, 37